How to cite: Angew. Chem. Int. Ed. 2023, e202305978
doi.org/10.1002/anie.202305978

2D Materials Hot Paper

A Thiophene Backbone Enables Two-Dimensional Poly(arylene vinylene)s with High Charge Carrier Mobility

Yamei Liu[+], Heng Zhang[+], Hongde Yu[+], Zhongquan Liao, Silvia Paasch, Shunqi Xu, Ruyan Zhao, Eike Brunner, Mischa Bonn, Hai I. Wang,* Thomas Heine, Mingchao Wang,* Yiyong Mai,* and Xinliang Feng**

Abstract: Linear conjugated polymers have attracted significant attention in organic electronics in recent decades. However, despite intrachain π-delocalization, interchain hopping is their transport bottleneck. In contrast, two-dimensional (2D) conjugated polymers, as represented by 2D π-conjugated covalent organic frameworks (2D *c*-COFs), can provide multiple conjugated strands to enhance the delocalization of charge carriers in space. Herein, we demonstrate the first example of thiophene-based 2D poly(arylene vinylene)s (PAVs, **2DPAV-BDT-BT** and **2DPAV-BDT-BP**, BDT = benzodithiophene, BT = bithiophene, BP = biphenyl) via Knoevenagel polycondensation. Compared with **2DPAV-BDT-BP**, the fully thiophene-based **2DPAV-BDT-BT** exhibits enhanced planarity and π-delocalization with a small band gap (1.62 eV) and large electronic band dispersion, as revealed by the optical absorption and density functional calculations. Remarkably, temperature-dependent terahertz spectroscopy discloses a unique band-like transport and outstanding room-temperature charge mobility for **2DPAV-BDT-BT** (65 $cm^2 V^{-1} s^{-1}$), which far exceeds that of the linear PAVs, **2DPAV-BDT-BP**, and the reported 2D *c*-COFs in the powder form. This work highlights the great potential of thiophene-based 2D PAVs as candidates for high-performance opto-electronics.

Introduction

Linear π-conjugated polymers are excellent semiconductor materials due to their structural versatility and tunable energy levels, coupled with tailorable electronic and optical properties.[1] In particular, polythiophene and its derivatives (Scheme 1a) have attracted considerable attention in organic field-effect transistors and organic photovoltaics[2] due to their easy synthesis and the following merits for enhanced charge transport: (1) the high polarizability of sulfur electrons in the thiophene rings enables a variety of intra- and inter-molecular interactions[3] e.g., sulfur-sulfur interactions, π-π stacking, etc. and stabilizes the conjugated polymer chain; (2) the structural versatility of thiophene motifs confers tunable photo-/electroactivity and band gap; (3) the planar thiophene-based polymer backbone strengthens parallel *p*-orbital interactions and thus π-conjugation.[4] Nevertheless, the charge transport performances achieved so far in linear conjugated polymers are still inadequate for high-performance organic electronics: the charge carriers are delocalized only along the linear backbone, and the hopping between adjacent polymer chains limits the delocalization of charge carriers in space.[5]

[*] Y. Liu,[+] Prof. Y. Mai
School of Chemistry and Chemical Engineering, Frontiers Science Center for Transformative Molecules, Shanghai Key Laboratory of Electrical Insulation and Thermal Ageing, Shanghai Jiao Tong University
800 Dongchuan Road, Shanghai 200240 (China)
E-mail: mai@sjtu.edu.cn

Y. Liu,[+] Dr. H. Yu,[+] Dr. S. Paasch, Dr. S. Xu, Dr. R. Zhao, Prof. E. Brunner, Prof. T. Heine, Dr. M. Wang, Prof. X. Feng
Center for Advancing Electronics Dresden (cfaed) and Faculty of Chemistry and Food Chemistry, Technische Universität Dresden
Mommsenstrasse 4, 01062 Dresden (Germany)
E-mail: shunqi.xu@tu-dresden.de
mingchao.wang@tu-dresden.de
xinliang.feng@tu-dresden.de

H. Zhang,[+] Prof. M. Bonn, Dr. H. I. Wang
Max Planck Institute for Polymer Research
Ackermannweg 10, 55128 Mainz (Germany)
E-mail: wanghai@mpip-mainz.mpg.de

Dr. Z. Liao
Fraunhofer Institute for Ceramic Technologies and Systems (IKTS)
01109 Dresden (Germany)

Prof. T. Heine
Helmholtz-Zentrum Dresden-Rossendorf, Forschungsstelle Leipzig
04318 Leipzig (Germany)
and
Department of Chemistry, Yonsei University
Seoul 03722 (Korea)

Prof. X. Feng
Max Planck Institute of Microstructure Physics
Weinberg 2, 06120 Halle (Germany)

[+] These authors contributed equally to this work.

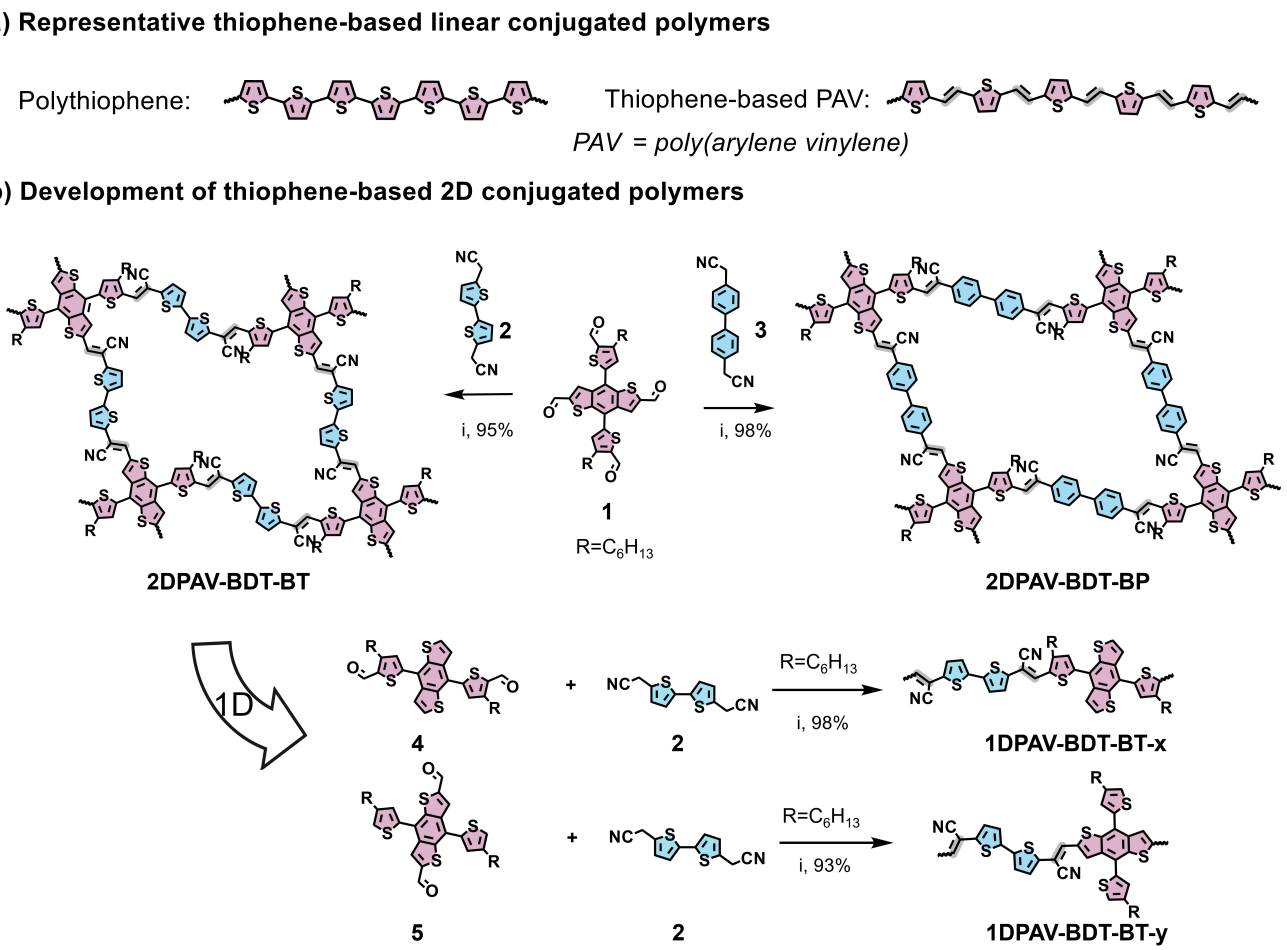

Scheme 1. Thiophene-based conjugated polymers. (a) Representative thiophene-based linear conjugated polymers. (b) Schematic synthesis of **2DPAV-BDT-BT**, **2DPAV-BDT-BP**, **1DPAV-BDT-BT-x** and **1DPAV-BDT-BT-y**. Reaction condition i: NH_4OAc, dioxane, 120 °C, 3 days.

The extension of π-conjugation in conjugated polymers from one-dimensional (1D) to two-dimensional (2D) can, in principle, provide multiple strands for charge transport, which may significantly improve the transport efficiency.[4,5b,6] 2D conjugated polymers, as represented by 2D π-conjugated covalent organic frameworks[7] (2D *c*-COFs), consist of multiple polymer strands linked by conjugated linkages (e.g., imine,[8] pyrazine,[9] vinylene,[10] etc.) and exhibit extended in-plane π-conjugation. In particular, crystalline 2D poly(arylene vinylene)s (2D PAVs, e.g., 2D poly(phenylene vinylene)s, also referred to as vinylene- or sp^2-carbon-linked 2D *c*-COFs), developed by Knoevenagel,[10–11] Aldol-type,[12] Horner–Wadsworth–Emmons[13] or Wittig[14] polycondensation, demonstrate π-conjugation/delocalization far beyond that of imine- or pyrazine-linked 2D polymer networks. Consequently, 2D PAVs are emerging semiconductor candidates for optoelectronics with reported mobility values as high as ~20 $cm^2 V^{-1} s^{-1}$.[15] Moreover, engineering the polymer framework with planar and π-extended molecular units such as phthalocyanine,[9a,16] porphyrin[17] and thiophene derivatives[18] enhances the π-conjugation and π–π interactions thus facilitating the charge transfer. Nevertheless, the reported 2D poly(phenylene vinylene)s are yet limited by inefficient 2D conjugation, as revealed by the weak in-plane dispersion in the energy band diagram.[10,14] We consider that the incorporation of highly planar, polarizable, and electron-rich thiophene units[18b,19] into the 2D PAV backbones would further enhance the charge carrier mobility[20] and potentially lead to unique electronic structures (e.g., Dirac cones,[21] anisotropic charge transport,[22] etc.), which are largely unexplored.

Herein, we demonstrate the first example of thienyl-benzodithiophene (abbreviated as thienyl-BDT)-based 2D PAVs (termed as **2DPAV-BDT-X**, with X=BT or BP bridged by bithiophene or biphenyl unit, respectively, displayed in Scheme 1b), showing the unique band-like transport and excellent charge mobility. Rhombic-shaped **2DPAV-BDT-Xs** were synthesized via an ammonium acetate (NH_4OAc)-catalyzed Knoevenagel 2D polycondensation of 4,8-bis(5-formyl-4-hexylthiophen-2-yl)benzo[1,2-b:4,5-b′]dithiophene-2,6-dicarbaldehyde (**1**) and (2,2′-([2,2′-bithiophene]-5,5′-diyl) diacetonitrile (**2**) or 2,2′-(biphenyl-4,4′-diyl) diacetonitrile (**3**) as polycrystalline powder samples. In addition, two thienyl-BDT-based 1D PAVs (**1DPAV-BDT-BT-x** and **1DPAV-BDT-BT-y**) were also synthesized. Compared with **2DPAV-BDT-BP**, the fully thiophene-based **2DPAV-BDT-BT** exhibits enhanced pla-

narity and π-delocalization with reduced band gap (1.62 vs. 1.90 eV) and large electronic band dispersion (and thus small charge effective mass, 0.1 vs. 0.24 m_e), as revealed by the optical absorption and density functional theory (DFT) calculations. Remarkably, ultrafast terahertz (THz) spectroscopy reveals an outstanding charge carrier mobility of ~65 $cm^2 V^{-1} s^{-1}$ for **2DPAV-BDT-BT**, which is superior to **2DPAV-BDT-BP**, **1DPAV-BDT-BT-x** and **1DPAV-BDT-BT-y** as well as the previously reported 2D *c*-COFs in the powder form. Furthermore, temperature-dependent measurements show that the photoconductivity and the inferred charge scattering time increase with decreasing temperature in **2DPAV-BDT-BT**, suggesting an intrinsic band-like transport behavior.

Results and Discussion

Thienyl-BDT was chosen as the building monomer because of its large π-conjugated system[2] and C_2 symmetry toward thiophene-based 2D conjugated polymer networks. To examine the reactivity of thienyl-BDT in Knoevenagel polycondensation, we synthesized **1DPAV-BDT-BT-x** and **1DPAV-BDT-BT-y** from 5,5′-(benzo[1,2-b:4,5-b′]dithiophene-4,8-diyl)bis(3-hexylthiophene-2-carbaldehyde) (**4**) or 4,8-bis(4-hexylthiophen-2-yl)benzo[1,2-b:4,5-b′]dithiophene-2,6-dicarbaldehyde (**5**) and **2** with NH_4OAc as the catalyst and dioxane as the solvent in a sealed glass ampoule at 120 °C for 3 days in a high yield of 98 % and 93 %, respectively. The successful synthesis of 1D PAVs was confirmed by solid-state ^{13}C cross-polarization magic-angle spinning (CP-MAS) nuclear magnetic resonance (NMR) spectroscopy (Figures S1 and S2), mass spectrometry (with detectable molecular weight up to 10^4 g mol^{-1} and interval of 787 g mol^{-1} for the repeating unit of $C_{44}H_{38}N_2S_6$, Figure S3), and Fourier-transform infrared (FT-IR) spectroscopy (Figure S4). Under the same conditions, **2DPAV-BDT-Xs** were synthesized from **1** and **2** or **3** by Knoevenagel 2D polycondensation with isolated yields of 95 % and 98 %, respectively (Scheme 1b and Table S1).

Powder X-ray diffraction (PXRD) analysis demonstrates the crystalline nature of both 2D PAVs. As shown in Figure 1a, **2DPAV-BDT-BT** displays intense signals at 5.01°, 8.90°, 10.16°, 25.41° (black line), suggesting long-range order in the 2D plane. We then performed a multi-level computational chemistry workflow and thoroughly screened ~30,000 potential structural models via force field, density-functional based tight binding, and DFT methods in sequence (Figures S5–7) to explore the stacked structure of the as-synthesized **2DPAV-BDT-BT**. We found that one structural model matches very well with the experimental PXRD signals, which are assigned to (010), (110), (200), (001) reflections, respectively (Figure 1a, dark cyan line at the bottom). Pawley refinement was further conducted, providing R_{wp} and R_p values as low as 1.86 % and 1.31 %, respectively, with unit parameters of $a = 22.78$ Å, $b = 20.49$ Å and $c = 3.99$ Å (and $\alpha = 70.67°$, $\beta = 81.21°$, and $\gamma = 119.53°$). Similarly, **2DPAV-BDT-BP** displays PXRD signals corresponding to (010) and (001) crystallographic planes (Figure 1a blue line). Its unit parameters are $a = 24.39$ Å, $b = 21.73$ Å, and $c = 3.90$ Å (and $\alpha = 70.67°$, $\beta = 81.21°$, and $\gamma = 119.53°$). As shown in Figure 1b, c and Figure S8, **2DPAV-BDT-BT** maintains the preferred planarity (i.e., with strengthened π-conjugation), while **2DPAV-BDT-BP** presents considerable twist, which causes reduced crystallinity in the latter.

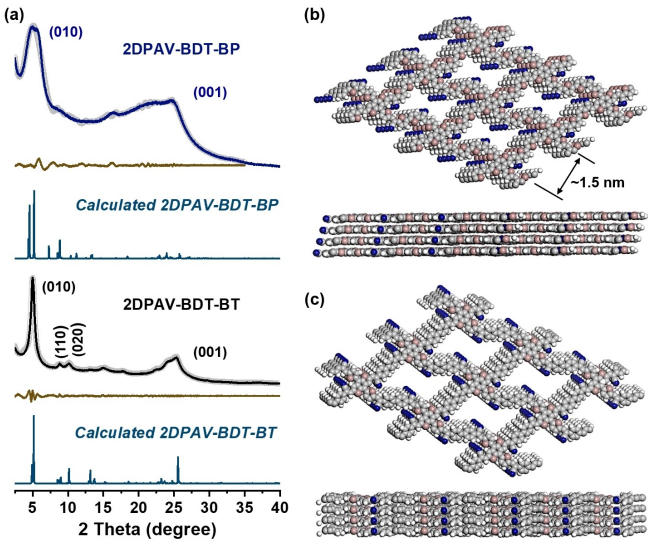

Figure 1. Crystal structure of **2DPAV-BDT-Xs**. (a) Experimental (black or blue line), Pawley refined (light grey dotted lines) and calculated PXRD (dark cyan lines) patterns as well as the refinement differences (brown lines) for **2DPAV-BDT-BT** and **2DPAV-BDT-BP**. (b, c) Top and side view of structural models of **2DPAV-BDT-BT** and **2DPAV-BDT-BP**, respectively. Alkyl chains were not depicted to clarify the topologies.

The formation of the vinylene linkage in **2DPAV-BDT-BT** ($^bC = {}^fC$-^eCN, b, f and e label the C atoms, Figure 2a, Figures S9 and S10) is identified by the solid-state ^{13}C CP-MAS NMR spectrum displaying ^{13}C signals at 138, 103 and 118 ppm (^bC, ^fC, ^eC, respectively) and other signals related to the thienyl-BDT and bithiophene moieties. No detectable aldehyde C peak can be found at over 170 ppm, indicating the successful polycondensation of monomers. FT-IR spectra indicate a shift of C≡N stretching vibrations in monomer **2** from ~2245 to ~2200 cm^{-1} in **2DPAV-BDT-BT** (Figure S11), which can be attributed to the extended conjugation in the latter. The peak at 1672 cm^{-1} belongs to the unreacted aldehydes at the edges.

The morphology was inspected by scanning electron microscopy (SEM), revealing aggregated flaky polycrystals in **2DPAV-BDT-BT** (Figure S12). High-resolution transmission electron microscopy (TEM) image manifests its periodic structure with a unit distance of ~1.5 nm at the nanoscale domain of 20×20 nm (Figure 2b), which agrees well with the shortest distance of parallel polymer strands (see details in Figure 1b and Figure S13). Similar to **2DPAV-BDT-BT**, the formation of **2DPAV-BDT-BP** is confirmed by solid-state ^{13}C CP-MAS NMR presented in Figure 2c and Figure S9 as well as other characterizations such as FT-IR, SEM, TEM, etc. in Figures S11, S14–S19.

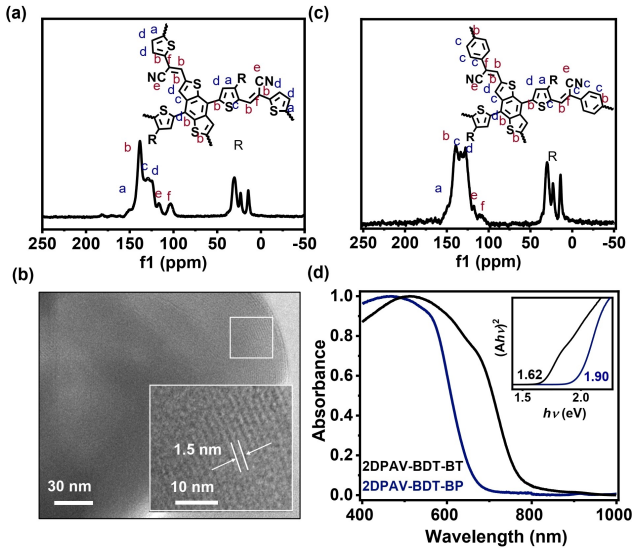

Figure 2. Component analysis and optical property of **2DPAV-BDT-Xs**. (a, c) Solid-state ^{13}C CP-MAS NMR spectra of **2DPVA-BDT-BT** and **2DPVA-BDT-BP**, respectively. (b) High-resolution TEM image of **2DPAV-BDT-BT**. The inset is the enlarged image. (d) UV/Visible-near IR absorption and Tauc plot of **2DPVA-BDT-BT** and **2DPVA-BDT-BP**.

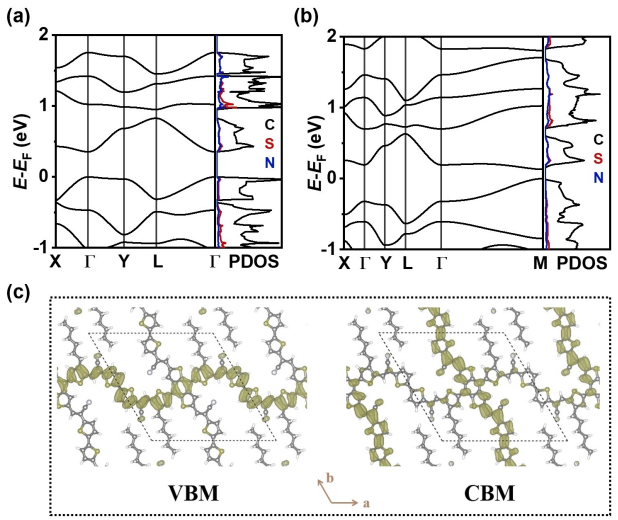

Figure 3. Electronic band structures and partial charge densities of **2DPAV-BDT-BT**. (a, b) Electronic band structures (left panel) and projected density of states (PDOS) (right panel) of monolayer and multilayer, respectively. (c) The partial charge densities at VBM and CBM of the multilayer system. The isosurface value is 0.0015 e/Bohr^3.

To investigate the optical properties of the **2DPAV-BDT-Xs**, we measured the absorbance of their dispersions in dimethylformamide in the UV/Visible and near-IR regions. **2DPAV-BDT-BT** clearly presents a narrower band gap, with the absorption onset starting from around 800 nm (Figure 2d). The optical band gap extracted from the Tauc plot is 1.62 eV, which is much smaller than those of **2DPAV-BDT-BP** (1.90 eV) and the reported 2D poly(phenylene vinylene)s (>2.0 eV).[10] This observation can be mainly attributed to the extended π-conjugation in **2DPAV-BDT-BT**.

The electronic band structures of the monolayer and layer-stacked **2DPAV-BDT-Xs** are calculated at the level of DFT (see Section 5 in the Supporting Information). As shown in Figure 3a, the **2DPAV-BDT-BT** monolayer is a semiconductor and exhibits significant dispersion in both the valance band (VB) and conduction band (CB), indicating the strong π-delocalization within the thienyl-BDT-based 2D backbone.[9a,15] Meanwhile, the layer-stacked **2DPAV-BDT-BT** retains dispersive VB and CB, and presents a diminished band gap due to the π-π stacking (Figure 3b). The strongly dispersive electronic bands correspond to the low effective masses of only 0.12 and 0.19 m_e for electrons and holes along *a* direction, respectively (Table S2). Notably, the out-of-plane effective mass values far exceed the in-plane ones (Table S2), indicating a favorable transport in the 2D plane. The electron-hole reduced effective mass (m^*) is calculated to be ca. 0.1 m_e in the layer-stacked **2DPAV-BDT-BT** (see details in Table S2) following:

$$\frac{1}{m^*} = \frac{1}{m_h^*} + \frac{1}{m_e^*}. \quad (1)$$

For comparison, we calculated the intrachain m^* of **1DPAV-BDT-BT-x** and **1DPAV-BDT-BT-y**, which are also ca. 0.1 m_e (structural models are presented in Figures S20 and S21). These low values indicate high mobility, but reflect the behavior of the ideal crystal without defects, domain walls, other scattering, or external factors. These factors likely affect the 1D conjugated polymers because a defect can only be circumvented by interchain hopping, whereas the 2D π-conjugated network is more robust.

We note that the dispersions of VB and CB diverge along ΓX and ΓY directions, indicative of an unprecedented in-plane anisotropic charge transport that has not yet been identified in the reported 2D *c*-COFs and conjugated 2D metal–organic frameworks.[6,9a,10,14,15,20,21,23] The delocalized electron density distribution at the VB maximum and CB minimum (VBM and CBM) fostering anisotropic transport is depicted in Figure 3c. Although **2DPAV-BDT-BP** possesses the same in-plane anisotropy (Figure S22–S23), in line with our expectation, the degree of conjugation is substantially reduced by the twisted biphenyl units, which results in a larger band gap and relatively weaker band dispersions, which is also reflected by the larger m^* of 0.24 m_e (Table S2). It is noteworthy that both **1DPAV-BDT-BT-x** and **1DPAV-BDT-BT-y** present, instead, isotropic charge transport (Figures S24 and S25), suggesting the crucial of dimensionality extension in achieving unique electronic structures.

To elucidate the effect of extended π-conjugation and π-delocalization pathways (2D vs. 1D) on the charge transport properties, we performed contact-free, optical pump-THz probe (OPTP) spectroscopy on the pelletized thienyl-BDT-based PAVs (see experimental details in Supporting Information). Freely propagating, single-cycle THz pulses (with ~1 ps duration) provide a contact-free manner for interrogating intrinsic charge transport in molecular materi-

als. In this approach, an ultrafast and coherent oscillating electric field drives a current, which in turn emits a terahertz field. The interference between the incident and emitted fields can be used to deduce the induced current and, thereby, the material's conductivity. To generate free charge carriers, an ultrashort optical laser pulse (400 nm, ~100 fs duration) is employed to excite interband transitions. The time- and frequency-dependent relative change of the transmitted THz field $-\Delta E/E$ through the photoexcited material is proportional to its photoconductivity (σ).[24] By varying the time delay between optical and THz pulses, we can measure the photoconductivity dynamics of **2DPAV-BDT-BT** and **2DPAV-BDT-BP**, as shown in Figure 4a (the photoconductivity dynamics of **1DPAV-BDT-BT-x** and **1DPAV-BDT-BT-y** were presented in Figure S26). These experiments were performed at the same absorbed fluences at room temperature. Similar to the previous reports,[9a,25] free carrier response dominates within the first ~2 ps for all the samples, followed by a fast decay due to the charge trapping or bound electron-hole pair (i.e., exciton) formation.[25]

The free carrier transport is further confirmed by frequency-resolved complex photoconductivity spectrum in Figure 4b measured at 0.5 ps after the peak of the photoconductivity dynamics in Figure 4a (see details of **2DPAV-BDT-BP**, **1DPAV-BDT-BT-x** and **1DPAV-BDT-BT-y** in Figure S27, see additional discussion with Figure S28). Such spectrum has been widely reported in organic polymers and polycrystalline materials where long-range free charge transport is limited microscopically by the conjugation irregularities and structural confinement such as grain boundaries. The conductivity spectra can be quantitatively described by the modified Drude model, i.e., the Drude–Smith (DS) model,[9a,15] which allows the extraction of the DS scattering time τ and confinement parameter c. We can further estimate the charge mobility in the dc limit with the knowledge of m^* following

$$\mu = \frac{e\tau}{m^*}(1+c). \tag{2}$$

Figure 4c compares the deduced charge mobilities from DS fitting and OPTP peak intensities of two PAVs. Overall, **2DPAV-BDT-BT** exhibits 2–4 times higher mobility than **2DPAV-BDT-BP**. This result is in line with our expectation and demonstrates that increasing the in-plane conjugation (**2DPAV-BDT-BT** vs. **2DPAV-BDT-BP**) and extending the π-delocalization pathways (**2DPAV-BDT-BT** vs. **1DPAV-BDT-BT-x/y**) improves the charge transport properties in conjugated polymers. Remarkably, **2DPAV-BDT-BT** shows the highest charge carrier mobility up to ~65 $cm^2 V^{-1} s^{-1}$, which represents, to the best of our knowledge, a record value among the thus-far developed 2D PAVs and *c*-COFs in powder form (Table S3).

To gain further insights into the charge transport properties, we performed temperature (T)-dependent photoconductivity studies on **2DPAV-BDT-BT** in vacuum with T ranging from 78 to 286 K (Figure S29). As summarized in Figure 4d, the OPTP peak intensities and extracted τ both increase by lowering T. This result is in line with the intrinsic band-like transport behavior in which lowering T reduces the electron-phonon scattering and thus enhances μ.[23] Yet, the relatively weak T-dependence observed here suggests that defect or impurity scattering sets one of the main constraints on the charge transport efficiency of **2DPAV-BDT-BT**.[6]

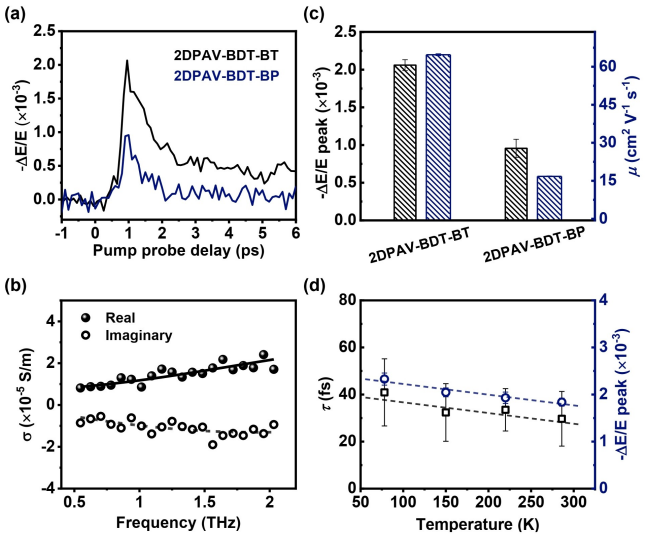

Figure 4. Time- and frequency-resolved THz photoconductivity. (a) Photoconductivity dynamics of **2DPAV-BDT-BT** and **2DPAV-BDT-BP** at room temperature following excitations at 400 nm with a fluence of 255 μJ cm^{-2}. (b) Frequency-resolved complex photoconductivity spectra of **2DPAV-BDT-BT**. The solid and dashed lines are Drude–Smith fits. (c) Comparison of the photoconductivity peak intensities in (a) and the charge mobilities from Drude–Smith fits. The details of **1DPAV-BDT-BT-x** and **1DPAV-BDT-BT-y** are shown in Table S3. (d) T-dependent scattering times and photoconductivity peaks of **2DPAV-BDT-BT**. The error bars for scattering time originate from the uncertainty of Drude–Smith fit. The error bars for the photoconductivity peak represent the standard errors calculated from ~30 measurements. The dashed lines are used to guide the eye.

Conclusion

In conclusion, we report the first crystalline fully thiophene-based 2D PAVs by Knoevenagel polycondensation. Theoretical calculations and experimental results demonstrate that a thiophene-based polymer backbone ensures sufficient π-conjugation, and the extended π-delocalization pathways enhance the charge transport effect. Benefiting from the planarity and extended π-conjugation, the achieved **2DPAV-BDT-BT** exhibits a narrow optical band gap, significant electronic band dispersion, and intrinsic band-like transport behavior, showing charge carrier mobility of up to ~65 $cm^2 V^{-1} s^{-1}$, which exceeds the reported 2D *c*-COFs in the powder form. Further structural design to strengthen 2D π-conjugation and the synthesis of highly crystalline and oriented 2D PAV films will be explored to develop 2D PAVs-based organic electronic devices.

Author Contributions

X.F., Y.M. and M.W. conceived and designed the project. Y.L. performed most experiments and interpreted the data. H.Z., M.B. and H.I.W. conducted the THz measurements and analyzed the data. H.Y. and T.H. contributed to the DFT calculations. Z.L. helped with TEM measurements. S.P. and E.B. performed the solid-state NMR measurements. S.X. and Y.L. designed the monomers and 2D PAVs. R.Z. contributed to helpful discussions. Y.L., Y.M., M.W. and X.F. co-wrote the manuscript with contributions from all co-authors.

Acknowledgements

This work was financially supported by ERC grant (T2DCP, No. 819698), DFG project (CRC 1415, No. 417590517), European Union's Horizon 2020 (PROGENY, No. 899205; Graphene Flagship Core3, No. 881603; EMERGE, No. 101008701), and Center for Advancing Electronics Dresden. Y.M.L. appreciates fellowship support from the Chinese Scholarship Council (CSC). Y.M. acknowledges the financial support from National Natural Science Foundation of China (52073173 and 22225501), and National Key R&D Program of China (2021YFB4001100). We thank Dresden Center for Nanoanalysis (DCN) for the use of facilities and Matthias Kluge for TGA measurement. We appreciate Dr. Yang Lu, Dr. Yannan Liu, Albrecht Wäntig and Shaik Ghouse for helpful discussions. H.Y. and T.H. acknowledge the Alexander von Humboldt Foundation for financial support and the Centre for Information Services and High Performance Computing (ZIH) at TU Dresden for the provided computational resources. The Instrumental Analysis Center at Shanghai Jiao Tong University is also acknowledged. Open Access funding enabled and organized by Projekt DEAL.

Conflict of Interest

The authors declare no conflict of interest.

Data Availability Statement

The data that support the findings of this study are available from the corresponding author upon reasonable request.

Keywords: 2D Conjugated COFs · 2D Poly(Arylene Vinylene)s · Band-Like Transport · Charge Mobility · Thiophene Backbone

[1] a) Y.-J. Cheng, S.-H. Yang, C.-S. Hsu, *Chem. Rev.* **2009**, *109*, 5868–5923; b) W. Niu, J. Ma, P. Soltani, W. Zheng, F. Liu, A. A. Popov, J. J. Weigand, H. Komber, E. Poliani, C. Casiraghi, J. Droste, M. R. Hansen, S. Osella, D. Beljonne, M. Bonn, H. I. Wang, X. Feng, J. Liu, Y. Mai, *J. Am. Chem. Soc.* **2020**, *142*, 18293–18298; c) H. Peng, S. Huang, D. Tranca, F. Richard, W. Baaziz, X. Zhuang, P. Samorì, A. Ciesielski, *ACS Nano* **2021**, *15*, 18580–18589; d) K. Jiang, J. Zhang, C. Zhong, F. R. Lin, F. Qi, Q. Li, Z. Peng, W. Kaminsky, S.-H. Jang, J. Yu, X. Deng, H. Hu, D. Shen, F. Gao, H. Ade, M. Xiao, C. Zhang, A. K. Y. Jen, *Nat. Energy* **2022**, *7*, 1076–1086.

[2] L. Zhu, M. Zhang, J. Xu, C. Li, J. Yan, G. Zhou, W. Zhong, T. Hao, J. Song, X. Xue, Z. Zhou, R. Zeng, H. Zhu, C.-C. Chen, R. C. I. MacKenzie, Y. Zou, J. Nelson, Y. Zhang, Y. Sun, F. Liu, *Nat. Mater.* **2022**, *21*, 656–663.

[3] K. Xiao, Y. Liu, T. Qi, W. Zhang, F. Wang, J. Gao, W. Qiu, Y. Ma, G. Cui, S. Chen, X. Zhan, G. Yu, J. Qin, W. Hu, D. Zhu, *J. Am. Chem. Soc.* **2005**, *127*, 13281–13286.

[4] X. Guo, M. Baumgarten, K. Müllen, *Prog. Polym. Sci.* **2013**, *38*, 1832–1908.

[5] a) F. Xu, J. Zhang, P. Zhang, X. Luan, Y. Mai, *Mater. Chem. Front.* **2019**, *3*, 2283–2307; b) A. M. Evans, M. J. Strauss, A. R. Corcos, Z. Hirani, W. Ji, L. S. Hamachi, X. Aguilar-Enriquez, A. D. Chavez, B. J. Smith, W. R. Dichtel, *Chem. Rev.* **2022**, *122*, 442–564.

[6] a) R. Dong, P. Han, H. Arora, M. Ballabio, M. Karakus, Z. Zhang, C. Shekhar, P. Adler, P. S. Petkov, A. Erbe, S. C. B. Mannsfeld, C. Felser, T. Heine, M. Bonn, X. Feng, E. Cánovas, *Nat. Mater.* **2018**, *17*, 1027–1032; b) S. Fu, E. Jin, H. Hanayama, W. Zheng, H. Zhang, L. Di Virgilio, M. A. Addicoat, M. Mezger, A. Narita, M. Bonn, K. Müllen, H. I. Wang, *J. Am. Chem. Soc.* **2022**, *144*, 7489–7496.

[7] a) B. Gole, V. Stepanenko, S. Rager, M. Grüne, D. D. Medina, T. Bein, F. Würthner, F. Beuerle, *Angew. Chem. Int. Ed.* **2018**, *57*, 846–850; b) A. C. Jakowetz, T. F. Hinrichsen, L. Ascherl, T. Sick, M. Calik, F. Auras, D. D. Medina, R. H. Friend, A. Rao, T. Bein, *J. Am. Chem. Soc.* **2019**, *141*, 11565–11571; c) L. Yao, A. Rodríguez-Camargo, M. Xia, D. Mücke, R. Guntermann, Y. Liu, L. Grunenberg, A. Jiménez-Solano, S. T. Emmerling, V. Duppel, K. Sivula, T. Bein, H. Qi, U. Kaiser, M. Grätzel, B. V. Lotsch, *J. Am. Chem. Soc.* **2022**, *144*, 10291–10300; d) X. Li, K. Zhang, G. Wang, Y. Yuan, G. Zhan, T. Ghosh, W. P. D. Wong, F. Chen, H.-S. Xu, U. Mirsaidov, K. Xie, J. Lin, K. P. Loh, *Nat. Synth.* **2022**, *1*, 382–392; e) J.-M. Seo, H.-J. Noh, J.-P. Jeon, H. Kim, G.-F. Han, S. K. Kwak, H. Y. Jeong, L. Wang, F. Li, J.-B. Baek, *J. Am. Chem. Soc.* **2022**, *144*, 19973–19980; f) C. Liu, Y. Jin, Z. Yu, L. Gong, H. Wang, B. Yu, W. Zhang, J. Jiang, *J. Am. Chem. Soc.* **2022**, *144*, 12390–12399.

[8] a) F. J. Uribe-Romo, J. R. Hunt, H. Furukawa, C. Klöck, M. O'Keeffe, O. M. Yaghi, *J. Am. Chem. Soc.* **2009**, *131*, 4570–4571; b) S.-Y. Ding, J. Gao, Q. Wang, Y. Zhang, W.-G. Song, C.-Y. Su, W. Wang, *J. Am. Chem. Soc.* **2011**, *133*, 19816–19822; c) S. Kandambeth, A. Mallick, B. Lukose, M. V. Mane, T. Heine, R. Banerjee, *J. Am. Chem. Soc.* **2012**, *134*, 19524–19527; d) H. Sahabudeen, H. Qi, B. A. Glatz, D. Tranca, R. Dong, Y. Hou, T. Zhang, C. Kuttner, T. Lehnert, G. Seifert, U. Kaiser, A. Fery, Z. Zheng, X. Feng, *Nat. Commun.* **2016**, *7*, 13461; e) C. Wu, Y. Liu, H. Liu, C. Duan, Q. Pan, J. Zhu, F. Hu, X. Ma, T. Jiu, Z. Li, Y. Zhao, *J. Am. Chem. Soc.* **2018**, *140*, 10016–10024; f) Y. Xie, J. Li, C. Lin, B. Gui, C. Ji, D. Yuan, J. Sun, C. Wang, *J. Am. Chem. Soc.* **2021**, *143*, 7279–7284.

[9] a) M. Wang, M. Ballabio, M. Wang, H.-H. Lin, B. P. Biswal, X. Han, S. Paasch, E. Brunner, P. Liu, M. Chen, M. Bonn, T. Heine, S. Zhou, E. Cánovas, R. Dong, X. Feng, *J. Am. Chem. Soc.* **2019**, *141*, 16810–16816; b) R. K. Dubey, M. Melle-Franco, A. Mateo-Alonso, *J. Am. Chem. Soc.* **2022**, *144*, 2765–2774.

[10] a) X. Zhuang, W. Zhao, F. Zhang, Y. Cao, F. Liu, S. Bi, X. Feng, *Polym. Chem.* **2016**, *7*, 4176–4181; b) E. Jin, M. Asada, Q. Xu, S. Dalapati, M. A. Addicoat, M. A. Brady, H. Xu, T. Nakamura, T. Heine, Q. Chen, D. Jiang, *Science* **2017**, *357*, 673–676.

[11] a) S. Wang, X.-X. Li, L. Da, Y. Wang, Z. Xiang, W. Wang, Y.-B. Zhang, D. Cao, *J. Am. Chem. Soc.* **2021**, *143*, 15562–15566;

b) Y. Su, Y. Wan, H. Xu, K.-I. Otake, X. Tang, L. Huang, S. Kitagawa, C. Gu, *J. Am. Chem. Soc.* **2020**, *142*, 13316–13321.
[12] a) H. Lyu, C. S. Diercks, C. Zhu, O. M. Yaghi, *J. Am. Chem. Soc.* **2019**, *141*, 6848–6852; b) T. Jadhav, Y. Fang, W. Patterson, C.-H. Liu, E. Hamzehpoor, D. F. Perepichka, *Angew. Chem. Int. Ed.* **2019**, *58*, 13753–13757; c) A. Acharjya, P. Pachfule, J. Roeser, F.-J. Schmitt, A. Thomas, *Angew. Chem. Int. Ed.* **2019**, *58*, 14865–14870; d) F. Meng, S. Bi, Z. Sun, B. Jiang, D. Wu, J.-S. Chen, F. Zhang, *Angew. Chem. Int. Ed.* **2021**, *60*, 13614–13620.
[13] D. L. Pastoetter, S. Xu, M. Borrelli, M. Addicoat, B. P. Biswal, S. Paasch, A. Dianat, H. Thomas, R. Berger, S. Reineke, E. Brunner, G. Cuniberti, M. Richter, X. Feng, *Angew. Chem. Int. Ed.* **2020**, *59*, 23620–23625.
[14] Y. Liu, S. Fu, D. L. Pastoetter, A. H. Khan, Y. Zhang, A. Dianat, S. Xu, Z. Liao, M. Richter, M. Yu, M. Položij, E. Brunner, G. Cuniberti, T. Heine, M. Bonn, H. I. Wang, X. Feng, *Angew. Chem. Int. Ed.* **2022**, *61*, e202209762.
[15] E. Jin, K. Geng, S. Fu, M. A. Addicoat, W. Zheng, S. Xie, J.-S. Hu, X. Hou, X. Wu, Q. Jiang, Q.-H. Xu, H. I. Wang, D. Jiang, *Angew. Chem. Int. Ed.* **2022**, *61*, e202115020.
[16] E. Jin, K. Geng, S. Fu, S. Yang, N. Kanlayakan, M. A. Addicoat, N. Kungwan, J. Geurs, H. Xu, M. Bonn, H. I. Wang, J. Smet, T. Kowalczyk, D. Jiang, *Chem* **2021**, *7*, 3309–3324.
[17] S. Wan, F. Gándara, A. Asano, H. Furukawa, A. Saeki, S. K. Dey, L. Liao, M. W. Ambrogio, Y. Y. Botros, X. Duan, S. Seki, J. F. Stoddart, O. M. Yaghi, *Chem. Mater.* **2011**, *23*, 4094–4097.
[18] a) H. Wei, J. Ning, X. Cao, X. Li, L. Hao, *J. Am. Chem. Soc.* **2018**, *140*, 11618–11622; b) S. Xu, H. Sun, M. Addicoat, B. P. Biswal, F. He, S. Park, S. Paasch, T. Zhang, W. Sheng, E. Brunner, Y. Hou, M. Richter, X. Feng, *Adv. Mater.* **2021**, *33*, 2006274; c) J.-P. Jeon, Y. J. Kim, S. H. Joo, H.-J. Noh, S. K. Kwak, J.-B. Baek, *Angew. Chem. Int. Ed.* **2023**, *62*, e202217416.
[19] Y. Wang, W. Hao, H. Liu, R. Chen, Q. Pan, Z. Li, Y. Zhao, *Nat. Commun.* **2022**, *13*, 100.
[20] M. Wang, R. Dong, X. Feng, *Chem. Soc. Rev.* **2021**, *50*, 2764–2793.
[21] G. Galeotti, F. De Marchi, E. Hamzehpoor, O. MacLean, M. Rajeswara Rao, Y. Chen, L. V. Besteiro, D. Dettmann, L. Ferrari, F. Frezza, P. M. Sheverdyaeva, R. Liu, A. K. Kundu, P. Moras, M. Ebrahimi, M. C. Gallagher, F. Rosei, D. F. Perepichka, G. Contini, *Nat. Mater.* **2020**, *19*, 874–880.
[22] W. Ma, P. Alonso-González, S. Li, A. Y. Nikitin, J. Yuan, J. Martín-Sánchez, J. Taboada-Gutiérrez, I. Amenabar, P. Li, S. Vélez, C. Tollan, Z. Dai, Y. Zhang, S. Sriram, K. Kalantar-Zadeh, S.-T. Lee, R. Hillenbrand, Q. Bao, *Nature* **2018**, *562*, 557–562.
[23] S. Ghosh, Y. Tsutsui, T. Kawaguchi, W. Matsuda, S. Nagano, K. Suzuki, H. Kaji, S. Seki, *Chem. Mater.* **2022**, *34*, 736–745.
[24] a) H. Zhang, E. Debroye, J. A. Steele, M. B. J. Roeffaers, J. Hofkens, H. I. Wang, M. Bonn, *ACS Energy Lett.* **2021**, *6*, 568–573; b) H. Zhang, E. Debroye, W. Zheng, S. Fu, L. D. Virgilio, P. Kumar, M. Bonn, H. I. Wang, *Sci. Adv.* **2021**, *7*, eabj9066.
[25] A. Tries, S. Osella, P. Zhang, F. Xu, C. Ramanan, M. Kläui, Y. Mai, D. Beljonne, H. I. Wang, *Nano Lett.* **2020**, *20*, 2993–3002.

Manuscript received: April 28, 2023
Accepted manuscript online: June 4, 2023
Version of record online: ■■, ■■

Research Articles

2D Materials

Y. Liu, H. Zhang, H. Yu, Z. Liao, S. Paasch, S. Xu,* R. Zhao, E. Brunner, M. Bonn, H. I. Wang,* T. Heine, M. Wang,* Y. Mai,* X. Feng* e202305978

A Thiophene Backbone Enables Two-Dimensional Poly(arylene vinylene)s with High Charge Carrier Mobility

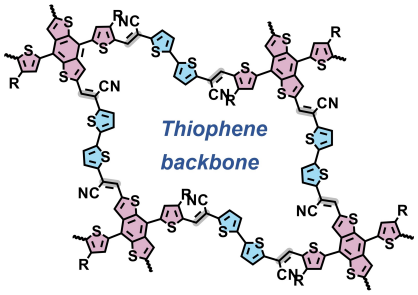

Band-like transport; μ = 65 cm^{2}V^{-1}s^{-1}

Crystalline, planar and fully thiophene-based two-dimensional poly(arylene vinylene) is developed for the first time via Knoevenagel polycondensation. It exhibits a narrow optical band gap and efficient π-delocalization for band-like transport and high charge carrier mobility.